Low-Iridium-Content IrNiTa Metallic Glass Films as Intrinsically Active Catalysts for Hydrogen Evolution Reaction

Zi-Jian Wang, Ming-Xing Li, Ji-Hao Yu, Xing-Bo Ge, Yan-Hui Liu,* and Wei-Hua Wang

Although various catalytic materials have emerged for hydrogen evolution reaction (HER), it remains crucial to develop intrinsically effective catalysts with minimum uses of expensive and scarce precious metals. Metallic glasses (MGs) or amorphous alloys show up as attractive HER catalysts, but have so far limited to material forms and compositions that result in high precious-metal loadings. Here, an $Ir_{25}Ni_{33}Ta_{42}$ MG nanofilm exhibiting high intrinsic activity and superior stability at an ultralow Ir loading of 8.14 µg cm^{-2} for HER in 0.5 M H_2SO_4 is reported. With an overpotential of 99 mV for a current density of 10 mA cm^{-2}, a small Tafel slope of 35 mV dec^{-1}, and high turnover frequencies of 1.76 and 19.3 H$_2$ s^{-1} at 50 and 100 mV overpotentials, the glassy film is among the most intrinsically active HER catalysts, outcompetes any reported MG, representative sulfides, and phosphides, and compares favorably with other precious-metal-containing catalysts. The outstanding HER performance of the $Ir_{25}Ni_{33}Ta_{42}$ MG film is attributed to the synergistic effect of the novel alloy system and amorphous structure, which may inspire the development of multicomponent alloys for heterogeneous catalysis.

Hydrogen has been proposed as an attractive energy carrier that could play a key role in sustainable energy systems.[1] Electrochemical water splitting offers a carbon-neutral way of producing hydrogen when driven by renewable energy sources of electricity.[1,2] As a fundamental component of this process, hydrogen evolution reaction (HER), $2H^+ + 2e^- \rightarrow H_2$, requires the use of a well-performing catalyst to achieve a high energetic efficiency.[2] At present, the most effective catalysts for HER in acidic electrolytes are still precious metals such as Pt and Ir.[2] Their low abundance and high cost have motivated great efforts to develop materials that could show similar HER properties but are far more cost-effective.[2]

Over the past decades, a number of Earth-abundant catalysts such as transition metal sulfides and phosphides were found to display HER activity approaching that of Pt or Ir in terms of the overpotential necessary to drive a specific current per geometric area (typically 10 mA cm^{-2}geo).[3] However, such high electrode activity generally arises from the enlarged surface areas or high catalyst loadings, underlining the insufficient intrinsic activity of these materials.[2] To develop low-cost catalysts of high intrinsic activity, two main strategies have been proposed to take better advantage of precious metals,[4] namely, to increase the surface area-to-volume ratio of a catalyst,[4] e.g., by reducing the dimension of Pt from bulk to thin film, monolayer, or even single atom,[5] and to alloy precious metals with nonprecious ones.[6] Although it can be expected that combining the two strategies would substantially reduce the use of precious metals without sacrificing efficiency, developing an alloy catalyst based on nonprecious metals for HER in acids with both high intrinsic activity and stability remains challenging.[2,4]

Metallic glasses (MGs), also known as amorphous alloys, are structurally disordered solids usually formed from molten alloy liquids by rapid quenching.[7] Unlike crystalline metals in which the constituent atoms reside at thermodynamic equilibrium, MGs are metastable materials in far-from-equilibrium states and exhibit a number of exotic mechanical and functional properties, e.g., high elastic limits, strength, toughness, and corrosion resistance.[7b–f] As a representative example, our recently developed bulk MGs in the Ir-Ni-Ta-(B) system can maintain a high strength of 3.7 GPa at 1000 K and even

Z.-J. Wang, Dr. M.-X. Li, J.-H. Yu, Prof. Y.-H. Liu, Prof. W.-H. Wang
Institute of Physics
Chinese Academy of Sciences
Beijing 100190, China
E-mail: yanhui.liu@iphy.ac.cn

Z.-J. Wang, J.-H. Yu, Prof. W.-H. Wang
School of Physical Sciences
University of Chinese Academy of Sciences
Beijing 100049, China

Dr. M.-X. Li, Prof. Y.-H. Liu, Prof. W.-H. Wang
Songshan Lake Materials Laboratory
Dongguan, Guangdong 523808, China

Prof. X.-B. Ge
School of Chemistry and Chemical Engineering
Southwest Petroleum University
Chengdu 610500, China

Prof. Y.-H. Liu
Center of Materials Science and Optoelectronics Engineering
University of Chinese Academy of Sciences
Beijing 100049, China

Prof. Y.-H. Liu, Prof. W.-H. Wang
Beijing Advanced Innovation Center for Materials Genome Engineering
University of Science and Technology Beijing
Beijing 100083, China

The ORCID identification number(s) for the author(s) of this article can be found under https://doi.org/10.1002/adma.201906384.

1906384 (1 of 7)

withstand the corrosion of aqua regia.[8] Despite that MGs have been demonstrated as appealing catalysts for a variety of reactions since 1980s,[9] it is only recently that a few MGs have been used to catalyze HER in acidic solutions, most of which are limited to material forms and compositions that result in ultrahigh precious metal loadings.[10] Therefore, new MG alloys and fabrication methods are required to further tap the potential of MGs for HER.

Here, we report a low-iridium-content $Ir_{25}Ni_{33}Ta_{42}$ (at% throughout this paper) MG film of nanometer thickness as an intrinsically active and highly stable HER catalyst in 0.5 M H_2SO_4. The film was fabricated by ion-beam deposition (IBD) on Si substrate. Its intrinsic activity is higher than any reported MG, representative sulfides, and phosphides, and compares favorably with other precious-metal-containing catalysts. We ascribe the excellent HER performance of the $Ir_{25}Ni_{33}Ta_{42}$ MG film to the synergistic effect of the novel alloy system and amorphous structure. This understanding may provide further

impetus for designing multicomponent alloys as heterogeneous catalysts.

The fabrication of a binder-free $Ir_{25}Ni_{33}Ta_{42}/Si$ electrode by the IBD method is illustrated in **Figure 1**a. An energetic beam of argon ions generated by the deposition ion source is directed toward the $Ir_{35}Ni_{25}Ta_{40}$ alloy sputtering target that was made by arc-melting followed by copper-mold casting. We chose this alloy as the target for its excellent glass-forming ability, thermal, and chemical stability.[8] During deposition, atoms are sputtered from the target surface and condensed as a thin film onto the Si substrate that has been cleaned by the assisted ion source. This IBD method is not only facile and scalable, but also can produce integrated electrodes as it allows straightforward deposition of various catalytic materials on a wide range of commercially available substrates such as carbon paper, carbon cloth, and metal foil or mesh. The film composition is determined to be $Ir_{25}Ni_{33}Ta_{42}$ by the energy-dispersive X-ray spectroscopy (EDX) spectrum of an approximately 1 µm thick freestanding
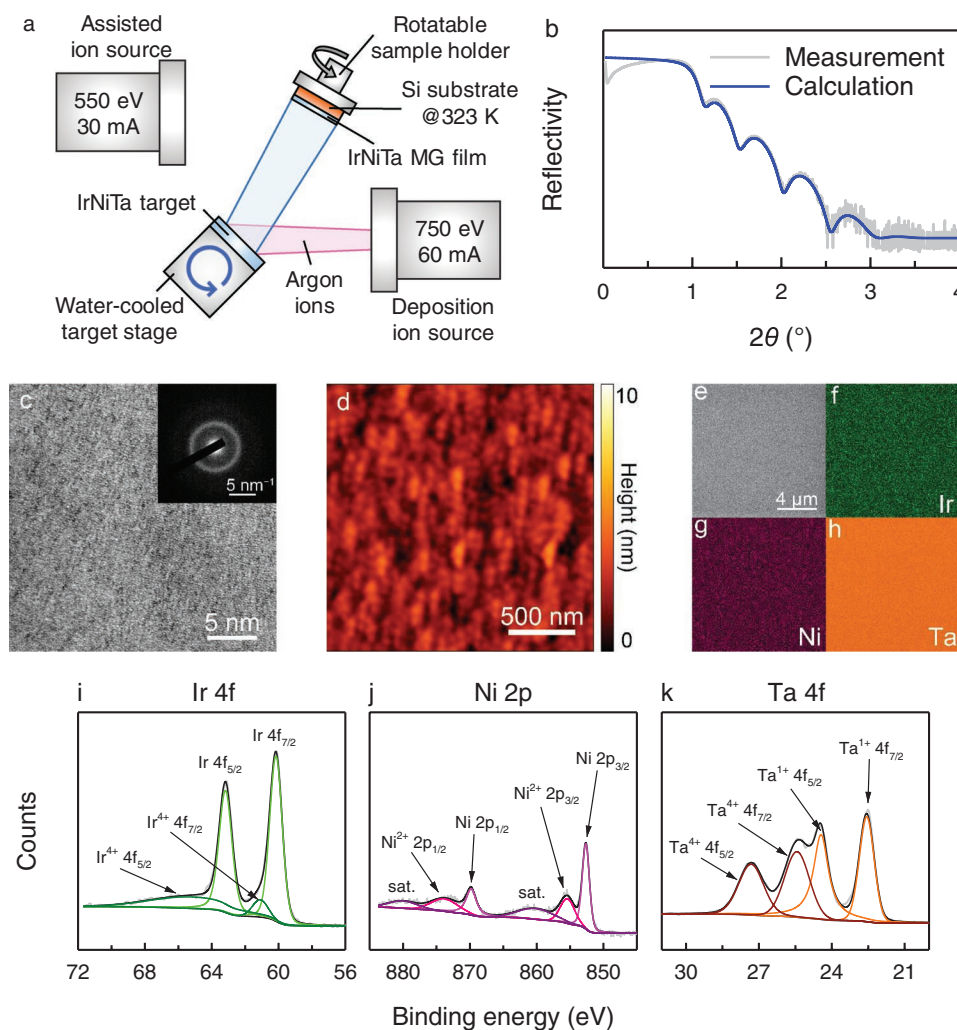
Figure 1. Fabrication and characterization of the $Ir_{25}Ni_{33}Ta_{42}$ MG film. a) Schematic diagram illustrating deposition of the $Ir_{25}Ni_{33}Ta_{42}$ MG film on Si substrates. b) Measured and calculated XRR data of the $Ir_{25}Ni_{33}Ta_{42}$ MG film on Si substrates. The film thickness is determined to be 15 nm. c) HRTEM image and its corresponding SAED pattern (inset) of the as-deposited $Ir_{25}Ni_{33}Ta_{42}$ MG film. d) AFM topography of the $Ir_{25}Ni_{33}Ta_{42}$ MG film surface. e–h) SEM morphology and EDX elemental mappings of the $Ir_{25}Ni_{33}Ta_{42}$ MG film. i–k) XPS spectra of Ir 4f (i), Ni 2p (j), and Ta 4f (k) of the $Ir_{25}Ni_{33}Ta_{42}$ MG film surface before electrochemical measurements. The satellite peaks for Ni^{2+} 2p are denoted as "sat." in (j).

**ADVANCED
SCIENCE NEWS**

www.advancedsciencenews.com

**ADVANCED
MATERIALS**

www.advmat.de

film (Figure S1, Supporting Information). The different compositions between the film and alloy target arise from different sputtering yields of Ir, Ni, and Ta elements.[11]

The thickness of the $Ir_{25}Ni_{33}Ta_{42}$ film deposited under ion beam energy of 750 eV and current of 60 mA for 2 min was determined to be 15 nm by fitting the X-ray reflectivity (XRR) curve (Figure 1b). As shown in Figure S2 in the Supporting Information, the X-ray grazing incidence diffraction pattern of the as-deposited $Ir_{25}Ni_{33}Ta_{42}$ film under the same deposition rate of 7.5 nm min^{-1} only shows a broad hump without any sharp Bragg peaks, indicating that the film is of a fully amorphous structure.[7d] This was further confirmed by the high-resolution transmission electron microscopy (HRTEM) image that exhibits a maze-like pattern and its corresponding selected area electron diffraction (SAED) pattern that features a diffuse halo-ring (Figure 1c).[7d]

In distinct contrast to many studies in which the enhancement of catalytic activity relies on an increased surface area by creating nanostructures on the surface, the $Ir_{25}Ni_{33}Ta_{42}$ MG film displays a surface that is almost atomically flat. Figure 1d shows its surface topography characterized by atomic force microscopy (AFM). As can be seen, the film has a very smooth surface without any notable structural features. The root mean square roughness is about 0.73 nm, only two to three atomic layers on average. The roughness factor, defined as the ratio between the electrochemical active surface area (ECSA) and geometric area of the scanned region (2×2 μm^2),[12] is essentially 1 cm$^2_{ECSA}$ cm$^{-2}_{geo}$. The nearly atomically flat surface of the $Ir_{25}Ni_{33}Ta_{42}$ MG film can greatly facilitate the evaluation of its intrinsic activity.
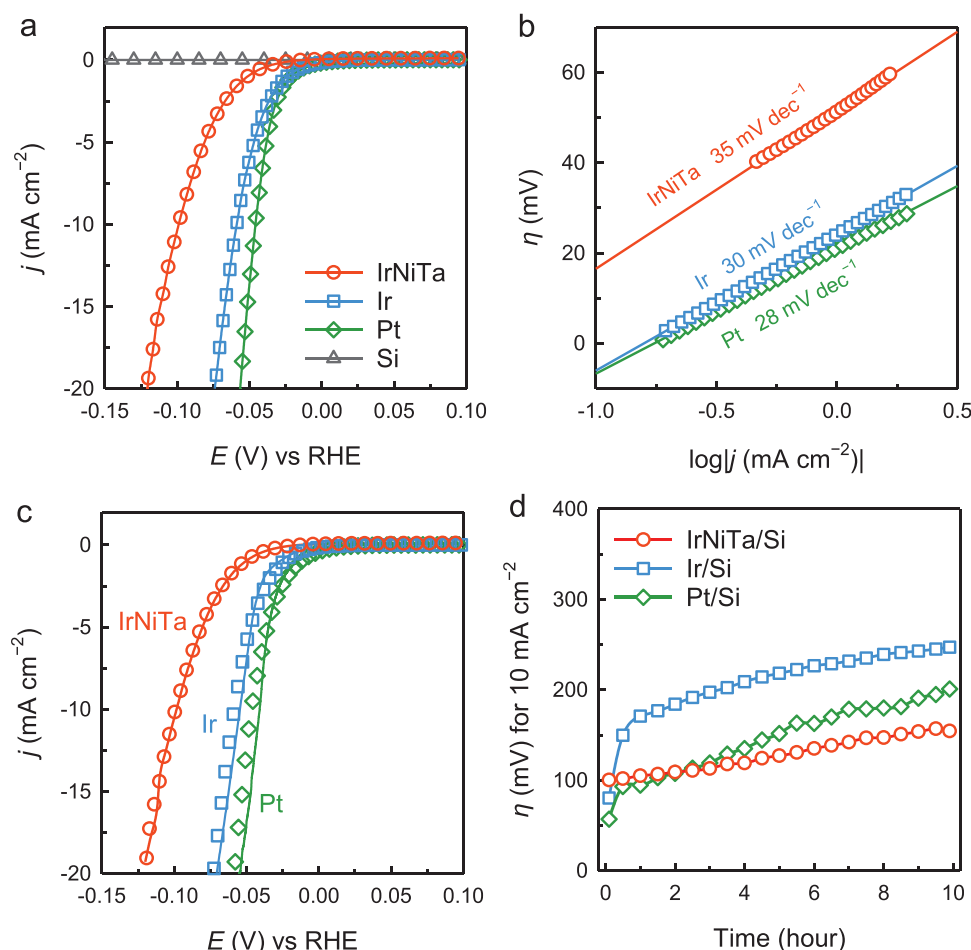
The scanning electron microscopy (SEM) image and its corresponding EDX elemental mappings (Figure 1e–h) reveal that the flat $Ir_{25}Ni_{33}Ta_{42}$ MG film is chemically homogenous as the distribution of Ir, Ni, and Ta elements is uniform. We also performed X-ray photoelectron spectroscopy (XPS) to investigate the chemical state of the $Ir_{25}Ni_{33}Ta_{42}$ MG film surface before electrochemical measurements (Figure 1i–k). The peaks at 60.16 and 63.18 eV are assigned to metallic Ir $4f_{7/2}$ and $4f_{5/2}$, respectively (Figure 1i), and the peaks with binding energies of 852.62 and 869.81 eV are indicative of metallic Ni species (Figure 1j).[13] It can be judged from the relative intensity that the surface Ir and Ni mainly exist in their metallic forms. In contrast, the XPS spectrum of Ta 4f (Figure 1k) is deconvoluted into four peaks that could be assigned to Ta^{1+} $4f_{7/2}$ (22.56 eV), Ta^{1+} $4f_{5/2}$ (24.44 eV), Ta^{4+} $4f_{7/2}$ (25.43 eV), and Ta^{4+} $4f_{5/2}$ (27.32 eV).[14] The strong oxidation tendency and low electronegativity of Ta could account for the absence of its metallic form.[15] There are also minor oxidized Ir and Ni species on the surface due to slight surface oxidation which is inevitable to the fresh sample during sample transfer. With a thickness of 15 nm and an estimated density of 16.19 g cm^{-3}, the Ir loading of the as-deposited $Ir_{25}Ni_{33}Ta_{42}$ MG film is calculated to be 8.14 μg cm^{-2} (Table S1, Supporting Information).

The electrocatalytic HER activity of the $Ir_{25}Ni_{33}Ta_{42}$/Si electrode was evaluated in 0.5 M H_2SO_4 at a scan rate of 2 mV s^{-1} in a two-compartment three-electrode setup. For comparison, Ir/Si electrode (Ir loading: 24.92 μg cm^{-2}) and Pt/Si electrode (Pt loading: 35.85 μg cm^{-2}) were also examined along with a bare Si electrode. The Ir/Si and Pt/Si electrodes were prepared

under the same deposition condition as that for the $Ir_{25}Ni_{33}Ta_{42}$/Si electrode. Both of the as-deposited Ir and Pt films have a thickness and roughness similar to that of the $Ir_{25}Ni_{33}Ta_{42}$ MG film (Figures S3 and S4 and Table S1, Supporting Information). **Figure 2**a shows the *iR*-corrected polarization curves of these electrodes on the reversible hydrogen electrode (RHE) scale. As expected, the bare Si electrode has no detectable contribution to hydrogen evolution within the investigated potential window. For the Ir/Si electrode, the overpotential to reach a geometric current density of 10 mA cm^{-2} is 59 mV, while that for the Pt/Si electrode is 46 mV, consistent with a previous report.[16] It is remarkable that the $Ir_{25}Ni_{33}Ta_{42}$/Si electrode with an extremely flat surface only needs an overpotential of 99 mV to deliver 10 mA cm^{-2}. This performance is also highly reproducible, as illustrated by the polarization curves displayed in Figure S5 in the Supporting Information for three consecutive electrodes. More importantly, the small overpotential of 99 mV is far less than that of highly active phosphide films fabricated on Si substrates, e.g., CoP (202 mV),[12] MoP (237 mV),[12] Co$_2$P (310 mV), and Ni$_2$P (240 mV) (Figure S6, Supporting Information).[17] In addition, the overpotential of the $Ir_{25}Ni_{33}Ta_{42}$/Si electrode for a mass activity of 1.0 mA μg$^{-1}_{Pt \, or \, Ir}$ is only slightly higher than that of the Ir/Si and Pt/Si electrodes (Figure S7, Supporting Information). These results imply that the $Ir_{25}Ni_{33}Ta_{42}$ MG film may have a high intrinsic activity for HER in acids.

It is generally accepted that HER in acidic environment with one catalytic intermediate H* (where * denotes an active site on the electrode surface) may occur through the Volmer step (H$^+$ + e$^-$ + * → H*), followed by the Heyrovsky step (H* + H$^+$ + e$^-$ → H$_2$ + *) or the Tafel step (H* + H* → H$_2$ + 2*).[4,18] Although it remains challenging to elucidate the exact reaction mechanism on a catalyst surface, Tafel slope can help identify the rate-determining step, and may provide insights into the possible reaction pathways.[4,18] Figure 2b presents the Tafel plots (overpotential η vs logarithmic current density log|j|) for the $Ir_{25}Ni_{33}Ta_{42}$/Si, Ir/Si, and Pt/Si electrodes. The linear portions of the plots were fitted by Tafel equation to obtain the Tafel slopes.[4,18] As shown in Figure 2b, the Tafel slopes of the Ir/Si and Pt/Si electrodes are 30 and 28 mV dec^{-1}, respectively, which are consistent with the values reported in literature.[19] Surprisingly, the $Ir_{25}Ni_{33}Ta_{42}$/Si electrode also shows a small Tafel slope of 35 mV dec^{-1}. When the Volmer step, Heyrovsky step, or Tafel step is sluggish, the Tafel slope is 118, 39, or 30 mV dec^{-1}, respectively.[4,18] The 35 mV dec^{-1} Tafel slope of the $Ir_{25}Ni_{33}Ta_{42}$/Si electrode suggests that hydrogen desorption could be the rate-determining step after fast hydrogen adsorption. However, the precise reaction pathway on the $Ir_{25}Ni_{33}Ta_{42}$ MG surface cannot be precisely identified at present due to the multicomponent nature of the alloy.

In addition to activity, stability is another major concern for HER catalysts. The short-term stability of the $Ir_{25}Ni_{33}Ta_{42}$/Si electrode was assessed by performing accelerated cyclic voltammetry (CV) scans between +0.1 and −0.3 V versus RHE (not *iR*-corrected) and compared with that of the Ir and Pt films. Figure 2c shows that after 1000 cycles the polarization curves of the $Ir_{25}Ni_{33}Ta_{42}$/Si, Ir/Si, and Pt/Si electrodes are almost coincident with the initial ones. This implies that the $Ir_{25}Ni_{33}Ta_{42}$ MG is as stable as Ir and Pt under short-term

**ADVANCED
SCIENCE NEWS**

www.advancedsciencenews.com

**ADVANCED
MATERIALS**

www.advmat.de

Figure 2. Electrochemical HER activity and stability of the $Ir_{25}Ni_{33}Ta_{42}$/Si electrode in 0.5 M H_2SO_4, along with that for the Ir/Si and Pt/Si electrodes. a) Polarization curves and b) Tafel plots of the $Ir_{25}Ni_{33}Ta_{42}$/Si, Ir/Si and Pt/Si electrodes. c) Polarization curves of the $Ir_{25}Ni_{33}Ta_{42}$/Si, Ir/Si, and Pt/Si electrodes before (symbols) and after 1000 CV scans (lines) between +0.1 and −0.3 V versus RHE. d) Chronopotentiometry curves of the $Ir_{25}Ni_{33}Ta_{42}$/Si, Ir/Si, and Pt/Si electrodes showing the changes of overpotentials with time at a constant current density of 10 mA cm^{-2}.

startup–shutdown conditions. We further conducted chronopotentiometry to examine the long-term stability of these electrodes. Specifically, we monitored the overpotential change at a fixed current density of 10 mA cm^{-2} for 10 h. As shown in Figure 2d, within the first 1 h both of the Ir/Si and Pt/Si electrodes experience dramatic increase in the overpotential and this tendency continues afterward. After 10 h, the increase of overpotential is up to ≈250 mV for the Ir/Si electrode and ≈200 mV for the Pt/Si electrode. This phenomenon was also observed in previous studies.[10a,19,20] In contrast, the $Ir_{25}Ni_{33}Ta_{42}$/Si electrode only shows a slight and slow deactivation in the process, with an overpotential increase of only 50 mV after 10 h. Despite that Ir and Pt are more active in terms of overpotential at a current density of 10 mA cm^{-2} (Figure 2a,b), the better operation stability of the $Ir_{25}Ni_{33}Ta_{42}$ MG makes it more competitive for potential applications.

The overpotential increase of the $Ir_{25}Ni_{33}Ta_{42}$/Si electrode during chronopotentiometry can be primarily attributed to its atomically flat film morphology. As the flat metallic surface cannot remove the evolved hydrogen bubbles quickly and spontaneously (Figure S8, Supporting Information), some active

sites may be blocked from the electrolyte or even stripped off the electrode surface.[20] In addition, the slight deactivation of the $Ir_{25}Ni_{33}Ta_{42}$/Si electrode may also be associated with the changes in the chemical state of the $Ir_{25}Ni_{33}Ta_{42}$ MG film surface. We have reported that $Ir_{35}Ni_{25}Ta_{40}$ bulk MG is highly corrosion-resistant, showing no weight loss in aqua regia for more than 100 days.[8] This prominent characteristic also holds true for the $Ir_{25}Ni_{33}Ta_{42}$ MG film as it does not dissolve in aqua regia even after high-pressure digestion treatment at 453 K for 24 h in an autoclave for three times (Figure S9, Supporting Information). However, even though the surface of the $Ir_{25}Ni_{33}Ta_{42}$/Si electrode remains extremely flat (Figure S10, Supporting Information) and chemically homogenous (Figure S11, Supporting Information) after the chronopotentiometry, a decrease in Ni content (Table S2, Supporting Information) on the surface (Figure S12, Supporting Information) can be observed. In addition, the XPS spectra collected after the chronopotentiometry reveal that the consumption of metallic Ir and Ni on the surface exposes more oxidized species that are less active for HER, and the Ta^{4+} state becomes dominant with a substantial decrease in the Ta^{1+} state (Figure S12, Supporting Information).

**ADVANCED
SCIENCE NEWS**

www.advancedsciencenews.com

**ADVANCED
MATERIALS**

www.advmat.de
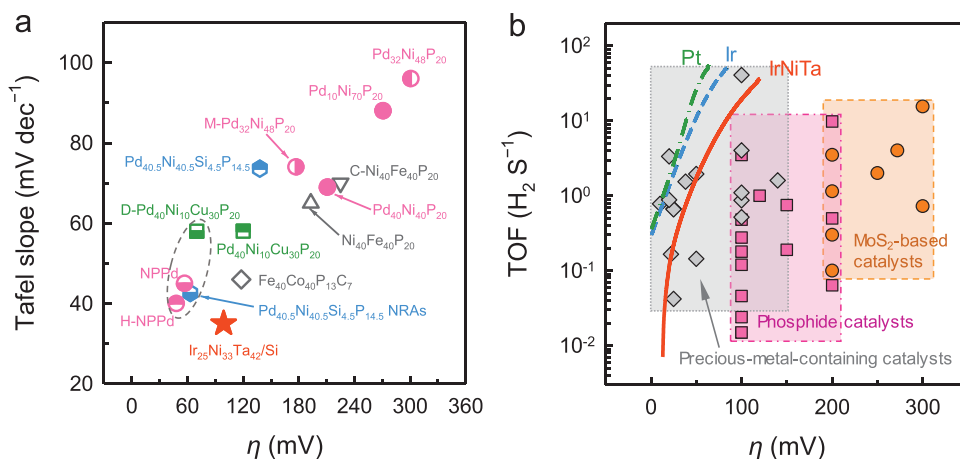
Figure 3. Comparison of the $Ir_{25}Ni_{33}Ta_{42}$ MG film with other catalysts for HER in 0.5 M H_2SO_4. a) Tafel slope versus the overpotential at 10 mA cm^{-2} for existing MG catalysts for HER, including as-spun (green top-filled square) and dealloyed (green bottom-filled square) $Pd_{40}Ni_{10}Cu_{30}P_{20}$ ribbons,[10a] $Pd_{40.5}Ni_{40.5}Si_{4.5}P_{14.5}$ plate and NRAs (blue hexagons),[10b] Pd-Ni-P MG or MG-based ribbons (pink circles),[10c,e] as-spun (black triangle) and crystallized (black inverted triangle) $Ni_{40}Fe_{40}P_{20}$ ribbons,[10c] and $Fe_{40}Co_{40}P_{13}C_7$ ribbon (black diamond).[10d] H-NPPd (Pd: 60.51 at%) with a hierarchical nanoporous structure is obtained from micropatterned $M-Pd_{32}Ni_{48}P_{20}$ ribbon by electrochemical dealloying, and NPPd (Pd: 80.82 at%) with a nanoporous structure is obtained from as-spun $Pd_{32}Ni_{48}P_{20}$ ribbon by the same electrochemical dealloying.[10e] MGs with overpotentials lower than that of the $Ir_{25}Ni_{33}Ta_{42}$/Si electrode are enclosed by a dashed ellipse. b) TOF values averaged over all surface sites of the $Ir_{25}Ni_{33}Ta_{42}$ MG film compared with the Ir film, Pt film, and other highly active HER catalysts, including molybdenum sulfide-based catalysts, transition metal phosphides, and precious-metal-containing catalysts. Detailed HER metrics of these catalysts are summarized in Table S3 in the Supporting Information.

Compared with previously reported MG catalysts (**Figure 3**a), the $Ir_{25}Ni_{33}Ta_{42}$ MG film exhibits both a low overpotential of 99 mV for 10 mA cm^{-2} and a small Tafel slope of 35 mV dec^{-1}. In fact, there are four MG-based electrodes (enclosed by the dashed ellipse in Figure 3a) that appear to exhibit lower overpotentials. However, surface structures may play dominant roles in such MG electrodes. For example, the H-NPPd electrode (Pd: 60.54 at%) with a micro/nano hierarchical porous structure is obtained by electrochemically dealloying the micropatterned $M-Pd_{32}Ni_{48}P_{20}$ ribbon, while the NPPD electrode (Pd: 80.82 at%) is obtained from the relatively flat $Pd_{32}Ni_{48}P_{20}$ ribbon after the same treatment.[10e] Similarly, the $Pd_{40.5}Ni_{40.5}Si_{4.5}P_{14.5}$ nanorod arrays (NRAs) and the $D-Pd_{40}Ni_{10}Cu_{30}P_{20}$ electrode are fabricated by micropatterning or dealloying of their respective precursor MG plate or ribbon.[10a,b] Therefore, it is evident that the low overpotentials of these complex-structured electrodes actually originate from the significantly increased surface areas rather than their intrinsic behaviors, because their relatively flat MG precursors show much worse HER performance (Figure 3a). Another noteworthy point is that P is an essential element in all the previously reported MG catalysts for HER in 0.5 M H_2SO_4 (Figure 3a). This is because P is not only necessary to guarantee the glass formation of these alloys,[7d] but also can promote HER by acting as negatively charged centers to trap protons at a low hydrogen coverage while facilitating hydrogen desorption at a high coverage.[3c] However, fabrication of P-containing MGs generally needs sophisticated procedure,[10c,21] and the chemical methods of synthesizing phosphides are difficult to obtain an amorphous structure.[3b,c] Furthermore, most of the MG catalysts containing P are Pd-rich alloys in the form of ribbons (Figure 3a). This form of materials inevitably results in extravagantly high Pd loadings that are about four orders of magnitude greater than the Ir loading of the $Ir_{25}Ni_{33}Ta_{42}$ MG film (see Supporting Information for an example). Therefore,

the $Ir_{25}Ni_{33}Ta_{42}$ MG film with an ultralow Ir loading is the most intrinsically active MG catalyst for HER in acids to date.

To quantify intrinsic activity, we estimated the turnover frequency (TOF), which is the number of hydrogen molecules evolved per second per site at a specific overpotential.[2b,c,3a] An atomically flat catalyst film with a roughness factor of 1 cm$^2_{ECSA}$ cm$^{-2}_{geo}$ provides an ideal model for the assessment of TOF as it facilitates estimation of the number of active sites on a catalyst surface.[12] The flat morphology is also beneficial for the determination of the inherent electrochemical double-layer capacitance of a catalyst.[12] As shown in Figure S13 in the Supporting Information, the specific capacitance of the flat $Ir_{25}Ni_{33}Ta_{42}$ MG film measured by performing CV scans in a non-Faradaic potential range at ten different rates is 45.72 ± 0.32 μF cm^{-2}. This value falls into the commonly used range of 20–60 μF cm^{-2} for a flat surface,[22] and can be used to improve the accuracy of TOF estimation for other $Ir_{25}Ni_{33}Ta_{42}$ MG catalysts with more complex structures. Prior to TOF calculation, the Faradaic efficiency of the $Ir_{25}Ni_{33}Ta_{42}$/Si electrode was measured by means of volume displacement.[22] For the $Ir_{25}Ni_{33}Ta_{42}$/Si electrode, essentially all the current contributes to hydrogen evolution because of a nearly 100% Faradaic efficiency (Figure S14, Supporting Information). To estimate the TOF of the $Ir_{25}Ni_{33}Ta_{42}$ MG film, we assumed that all the surface Ir, Ni, and Ta atomic sites are equally active (see Supporting Information for details). In fact, the calculation of the TOF of the $Ir_{25}Ni_{33}Ta_{42}$ MG film is insensitive to the exact surface composition as the three elements have similar atomic volumes (Figure S15, Supporting Information).

Figure 3b summarizes the estimated TOF of the $Ir_{25}Ni_{33}Ta_{42}$ MG, Ir, and Pt films, along with that of representative HER catalysts including sulfides, phosphides, and precious-metal-containing catalysts (see Table S3 for more information in the Supporting Information). The TOF values of the $Ir_{25}Ni_{33}Ta_{42}$

**ADVANCED
SCIENCE NEWS**

www.advancedsciencenews.com

**ADVANCED
MATERIALS**

www.advmat.de

MG film, e.g., 1.76 and 19.3 H$_2$ s^{-1} at overpotentials of 50 and 100 mV, respectively, are orders of magnitude greater than that of the catalysts based on molybdenum sulfides and transition metal phosphides, and outperforms many precious-metal-containing catalysts (Figure 3b). More importantly, the high intrinsic activity of the Ir$_{25}$Ni$_{33}$Ta$_{42}$ MG is achieved at an Ir loading of 8.14 µg cm^{-2} that is among the lowest for precious-metal-containing catalysts (Table S3, Supporting Information). It has been demonstrated that MGs can form in a broad composition range in the Ir-Ni-Ta system by sputtering deposition,[8] and their energy states can be widely tuned by a number of approaches.[23] Thus, further enhancement of intrinsic activity at a lower Ir loading is highly possible.

The excellent intrinsic activity and superior stability of the Ir$_{25}$Ni$_{33}$Ta$_{42}$ MG film indicate that it is a promising catalyst for HER in acids. Its outstanding performance can be attributed to the proper alloy system and amorphous structure. As HER consists of hydrogen adsorption and desorption, either too strong or too weak binding of hydrogen to the catalyst surface will decelerate the reaction.[24] A high activity is achieved only when the binding energy is appropriate,[24] as elaborated by the so-called "volcano plot" that serves as a valuable theoretical framework for catalyst design.[2b,6b,25] In the volcano plot for HER, precious metals (such as Pt and Ir) are located near the top, while early (such as Mo, Ti, and Ta) and late transition metals (such as Cu and Ni) are located on the opposite slopes of the volcano.[24a] Highly active binary alloy catalysts by combining elements on the opposite slopes, e.g., NiMo and CuTi alloys, have been successfully designed for HER in alkaline solutions, but often degrade rapidly in acidic electrolytes.[26] Our Ir-Ni-Ta alloy system demonstrates an effective strategy for designing acid-stable HER catalysts, i.e., combination of minor precious metals with early and late transition metals according to the volcano plot. The minor addition of precious metals not only greatly boosts the intrinsic activity but also alleviates the insufficient stability of alloys based on nonprecious metals in acids.

The amorphous structure of the Ir$_{25}$Ni$_{33}$Ta$_{42}$ MG film can also improve its activity and stability. In the disordered atomic structure of an MG, there are plenty of coordinatively unsaturated sites in association with higher energy states. Such characteristics have been proved helpful in promoting catalytic activity.[7d,f,9,27] As shown in Figure S16 in the Supporting Information, the Ir$_{25}$Ni$_{33}$Ta$_{42}$ MG film is far more active for HER than its crystalline counterpart. Moreover, in the absence of any conventional structural defects such as grain boundaries or dislocations, an MG is more corrosion-resistant than its crystalline counterpart, so that an enhanced catalytic stability in harsh environment can be achieved.[9,10c,d] Hence, it is the synergistic effect of choosing a proper alloy system and forming an amorphous alloy that leads to the outstanding activity and stability of the Ir$_{25}$Ni$_{33}$Ta$_{42}$ MG film. This alloy system also provides a platform for high-throughput computational or experimental screening to pinpoint the optimal composition with the highest intrinsic activity and stability at the lowest possible precious metal loading.[6b,28] It is reasonable to assume that our strategy can also be extended to the development of multicomponent alloys for other heterogeneous catalytic reactions.

In summary, a 15 nm thick Ir$_{25}$Ni$_{33}$Ta$_{42}$ MG film with an Ir loading as low as 8.14 µg cm^{-2} is grown on planar Si substrates

using a facile IBD method. The MG film shows high intrinsic activity and superior stability for HER in 0.5 M H$_2$SO$_4$. The Ir$_{25}$Ni$_{33}$Ta$_{42}$/Si electrode with a nearly atomically flat surface only requires an overpotential of 99 mV to drive a current density of 10 mA cm^{-2} and exhibits a small Tafel slope of 35 mV dec^{-1}. Moreover, with high TOF values of 1.76 and 19.3 H$_2$ s^{-1} at 50 and 100 mV, respectively, the Ir$_{25}$Ni$_{33}$Ta$_{42}$ MG film is among the most intrinsically active HER catalysts, outperforming any reported MG catalyst, representative molybdenum sulfide-based catalysts and transition metal phosphides, and comparing favorably with other precious-metal-containing catalysts. The outstanding HER performance of the Ir$_{25}$Ni$_{33}$Ta$_{42}$ MG film can be ascribed to the choice of the proper alloy system and amorphous structure. Our work not only provides a novel alloy system for HER in acids, but also bears importance for the design and development of multicomponent alloys as highly-performing heterogeneous catalysts.

Supporting Information

Supporting Information is available from the Wiley Online Library or from the author.

Acknowledgements

Conflict of Interest

The authors declare no conflict of interest.

Keywords

[1] J. A. Turner, *Science* **2004**, *305*, 972.
[2] a) I. Roger, M. A. Shipman, M. D. Symes, *Nat. Rev. Chem.* **2017**, *1*, 0003; b) Z. W. Seh, J. Kibsgaard, C. F. Dickens, I. Chorkendorff, J. K. Norskov, T. F. Jaramillo, *Science* **2017**, *355*, eaad4998; c) J. Kibsgaard, I. Chorkendorff, *Nat. Energy* **2019**, *4*, 430.
[3] a) J. D. Benck, T. R. Hellstern, J. Kibsgaard, P. Chakthranont, T. F. Jaramillo, *ACS Catal.* **2014**, *4*, 3957; b) J. F. Callejas, C. G. Read,

**ADVANCED
SCIENCE NEWS**

www.advancedsciencenews.com

**ADVANCED
MATERIALS**

www.advmat.de

C. W. Roske, N. S. Lewis, R. E. Schaak, *Chem. Mater.* **2016**, *28*, 6017; c) Y. Shi, B. Zhang, *Chem. Soc. Rev.* **2016**, *45*, 1529.

[4] a) M. Zeng, Y. G. Li, *J. Mater. Chem. A* **2015**, *3*, 14942; b) X. M. Li, X. G. Hao, A. Abudula, G. Q. Guan, *J. Mater. Chem. A* **2016**, *4*, 11973.

[5] a) D. V. Esposito, S. T. Hunt, Y. C. Kimmel, J. G. Chen, *J. Am. Chem. Soc.* **2012**, *134*, 3025; b) M. Li, Q. Ma, W. Zi, X. Liu, X. Zhu, S. F. Liu, *Sci. Adv.* **2015**, *1*, e1400268; c) L. Zhang, K. Doyle-Davis, X. L. Sun, *Energy Environ. Sci.* **2019**, *12*, 492.

[6] a) J. Greeley, M. Mavrikakis, *Nat. Mater.* **2004**, *3*, 810; b) J. Greeley, T. F. Jaramillo, J. Bonde, I. B. Chorkendorff, J. K. Norskov, *Nat. Mater.* **2006**, *5*, 909; c) C. Chen, Y. Kang, Z. Huo, Z. Zhu, W. Huang, H. L. Xin, J. D. Snyder, D. Li, J. A. Herron, M. Mavrikakis, M. Chi, K. L. More, Y. Li, N. M. Markovic, G. A. Somorjai, P. Yang, V. R. Stamenkovic, *Science* **2014**, *343*, 1339.

[7] a) W. Klement, R. H. Willens, P. Duwez, *Nature* **1960**, *187*, 869; b) A. L. Greer, *Science* **1995**, *267*, 1947; c) A. L. Greer, E. Ma, *MRS Bull.* **2007**, *32*, 611; d) Y. Q. Cheng, E. Ma, *Prog. Mater. Sci.* **2011**, *56*, 379; e) J. Schroers, *Phys. Today* **2013**, *66*, 32; f) E. Ma, *Nat. Mater.* **2015**, *14*, 547.

[8] M. X. Li, S. F. Zhao, Z. Lu, A. Hirata, P. Wen, H. Y. Bai, M. Chen, J. Schroers, Y. Liu, W. H. Wang, *Nature* **2019**, *569*, 99.

[9] a) A. Baiker, *Faraday Discuss. Chem. Soc.* **1989**, *87*, 239; b) J. Li, G. Doubek, L. McMillon-Brown, A. D. Taylor, *Adv. Mater.* **2019**, *31*, 1802120; c) Y. C. Hu, C. X. Sun, C. W. Sun, *ChemCatChem* **2019**, *11*, 2401; d) L. C. Zhang, Z. Jia, F. C. Lyu, S. X. Liang, J. Lu, *Prog. Mater. Sci.* **2019**, *105*, 100576.

[10] a) Y. C. Hu, Y. Z. Wang, R. Su, C. R. Cao, F. Li, C. W. Sun, Y. Yang, P. F. Guan, D. W. Ding, Z. L. Wang, W. H. Wang, *Adv. Mater.* **2016**, *28*, 10293; b) S. H. Gao, J. L. Jia, S. Q. Chen, H. W. Luan, Y. Shao, K. F. Yao, *RSC Adv.* **2017**, *7*, 27058; c) Y. W. Tan, F. Zhu, H. Wang, Y. Tian, A. Hirata, T. Fujita, M. W. Chen, *Adv. Mater. Interfaces* **2017**, *4*, 1601086; d) F. Zhang, J. Wu, W. Jiang, Q. Hu, B. Zhang, *ACS Appl. Mater. Interfaces* **2017**, *9*, 31340; e) S. S. Wang, N. Li, L. Liu, *Mater. Lett.* **2018**, *228*, 443.

[11] M. P. Seah, *Thin Solid Films* **1981**, *81*, 279.

[12] T. R. Hellstern, J. D. Benck, J. Kibsgaard, C. Hahn, T. F. Jaramillo, *Adv. Energy Mater.* **2016**, *6*, 1501758.

[13] A. V. Naumkin, A. Kraut-Vass, C. J. Powell, *NIST X-ray Photoelectron Spectroscopy Database*, Measurement Services Division of the National Institute of Standards and Technology (NIST) Technology Services, Gaithersburg, MD, USA **2008**.

[14] R. Simpson, R. G. White, J. F. Watts, M. A. Baker, *Appl. Surf. Sci.* **2017**, *405*, 79.

[15] M. Zier, S. Oswald, R. Reiche, K. Wetzig, *Anal. Bioanal. Chem.* **2003**, *375*, 902.

[16] J. Seok, J. H. Lee, S. Cho, B. Ji, H. W. Kim, M. Kwon, D. Kim, Y. M. Kim, S. H. Oh, S. W. Kim, Y. H. Lee, Y. W. Son, H. Yang, *2D Mater.* **2017**, *4*, 025061.

[17] C. G. Read, J. F. Callejas, C. F. Holder, R. E. Schaak, *ACS Appl. Mater. Interfaces* **2016**, *8*, 12798.

[18] X. Tian, P. Zhao, W. Sheng, *Adv. Mater.* **2019**, *31*, 1808066.

[19] M. Sheng, B. Jiang, B. Wu, F. Liao, X. Fan, H. Lin, Y. Li, Y. Lifshitz, S. T. Lee, M. Shao, *ACS Nano* **2019**, *13*, 2786.

[20] Y. J. Li, H. C. Zhang, T. H. Xu, Z. Y. Lu, X. C. Wu, P. B. Wan, X. M. Sun, L. Jiang, *Adv. Funct. Mater.* **2015**, *25*, 1737.

[21] a) A. J. Drehman, A. L. Greer, D. Turnbull, *Appl. Phys. Lett.* **1982**, *41*, 716; b) Y. He, R. B. Schwarz, J. I. Archuleta, *Appl. Phys. Lett.* **1996**, *69*, 1861; c) F. Hu, S. Zhu, S. Chen, Y. Li, L. Ma, T. Wu, Y. Zhang, C. Wang, C. Liu, X. Yang, L. Song, X. Yang, Y. Xiong, *Adv. Mater.* **2017**, *29*, 1606570.

[22] J. Kibsgaard, T. F. Jaramillo, *Angew. Chem.* **2014**, *126*, 14661; *Angew. Chem., Int. Ed. Engl.* **2014**, *53*, 14433.

[23] Y. H. Sun, A. Concustell, A. L. Greer, *Nat. Rev. Mater.* **2016**, *1*, 16039.

[24] a) S. Trasatti, *J. Electroanal. Chem. Interfacial Electrochem.* **1972**, *39*, 163; b) W. C. Sheng, M. Myint, J. G. G. Chen, Y. S. Yan, *Energy Environ. Sci.* **2013**, *6*, 1509.

[25] a) C. J. H. Jacobsen, S. Dahl, B. S. Clausen, S. Bahn, A. Logadottir, J. K. Norskov, *J. Am. Chem. Soc.* **2001**, *123*, 8404; b) A. J. Medford, A. Vojvodic, J. S. Hummelshoj, J. Voss, F. Abild-Pedersen, F. Studt, T. Bligaard, A. Nilsson, J. K. Norskov, *J. Catal.* **2015**, *328*, 36.

[26] a) J. R. McKone, B. F. Sadtler, C. A. Werlang, N. S. Lewis, H. B. Gray, *ACS Catal.* **2013**, *3*, 166; b) Q. Lu, G. S. Hutchings, W. Yu, Y. Zhou, R. V. Forest, R. Tao, J. Rosen, B. T. Yonemoto, Z. Cao, H. Zheng, J. Q. Xiao, F. Jiao, J. G. Chen, *Nat. Commun.* **2015**, *6*, 6567.

[27] G. Doubek, R. C. Sekol, J. Li, W. H. Ryu, F. S. Gittleson, S. Nejati, E. Moy, C. Reid, M. Carmo, M. Linardi, P. Bordeenithikasem, E. Kinser, Y. Liu, X. Tong, C. O. Osuji, J. Schroers, S. Mukherjee, A. D. Taylor, *Adv. Mater.* **2016**, *28*, 1940.

[28] a) P. J. McGinn, *Mater. Discovery* **2015**, *1*, 38; b) K. Sliozberg, D. Schafer, T. Erichsen, R. Meyer, C. Khare, A. Ludwig, W. Schuhmann, *ChemSusChem* **2015**, *8*, 1270; c) J. Y. Li, H. S. Stein, K. Sliozberg, J. B. Liu, Y. H. Liu, G. Sertic, E. Scanley, A. Ludwig, J. Schroers, W. Schuhmann, A. D. Taylor, *J. Mater. Chem. A* **2017**, *5*, 67; d) A. Ludwig, *npj Comput. Mater.* **2019**, *5*, 70.